

# Galaxy Statistics in Pencil-beam Surveys at High Redshifts

Joseph A. Muñoz<sup>\*</sup>, Hy Trac, and Abraham Loeb

*Harvard-Smithsonian Center for Astrophysics, 60 Garden St., MS 10, Cambridge, MA 02138, USA*

21 June 2024

## ABSTRACT

Surveys of faint galaxies at high redshifts often result in a “pencil-beam” geometry that is much longer along the line-of-sight than across the sky. We explore the effects of this geometry on the abundance and clustering of Lyman-break galaxies (LBGs) and Lyman- $\alpha$  emitters (LAEs) based on cosmological N-body simulations which adequately describe the nonlinear growth of structure on small scales. We find that the probability distribution of the LBG abundance is skewed toward low values since the narrow transverse dimension of the survey is more likely to probe underdense regions. Over a range that spans 1–2 orders of magnitude in galaxy luminosities, the variance in the number of objects differs from the commonly used analytic prediction and is not dominated by Poisson noise. Additionally, nonlinear bias on small scales results in a one-dimensional power spectrum of LAEs using a James Webb Space Telescope field-of-view that is relatively flat, markedly different from the expectation of linear perturbation theory. We discuss how these results may affect attempts to measure the UV background at high redshifts, estimate the relationship between halo mass and galaxy luminosity, and probe reionization by measuring the power-modulating effect of ionized regions.

**Key words:** cosmology: theory – cosmology: observations – early universe – large-scale structure of the universe – galaxies: high-redshift – galaxies: abundances

## 1 INTRODUCTION

Over the past few years, searches for Lyman-break galaxies (LBGs) and Lyman-alpha emitters (LAE) have revealed new populations of young, star-forming objects at redshift beyond  $z = 6$  (Stark et al. 2007a; Richard et al. 2008; Bouwens et al. 2008, 2009) that shed light on the star formation history at high redshifts and the sources responsible for cosmic reionization. In addition, evidence has been found for a population of massive, evolved systems around  $z = 5$  (Mobasher et al. 2005; Wiklind et al. 2008) that hints at an earlier period of higher star formation than has yet to be seen in surveys of bright LBGs and LAEs.

Theoretically, it is expected that the bulk of the star formation during reionization had taken place in less luminous galaxies than previously observed (Barkana & Loeb 2001; Wyithe & Loeb 2006). Dwarf galaxies are supposed to supply the bulk of the radiation that reionizes the Universe as well as provide the building blocks of the Milky Way and the possible birth place of globular clusters (Kravtsov & Gnedin 2005; Gnedin & Kravtsov 2006; Moore et al. 2006; Madau et al. 2008; Muñoz et al. 2009). Attempts to probe the faint end of the luminosity function have often sacrificed field-of-view for the sake of higher flux

sensitivity. Objects in the  $11.2 \text{ arcmin}^2$  Hubble Ultra Deep Field (HUDF), for example, can be seen in the  $z_{850}$  pass-band down to an apparent magnitude of about 29. In an even more extreme case, a single long-slit spectroscopic survey for gravitationally-lensed LAEs has a field-of-view of only about  $32 \text{ arcsec}^2$  (which is even smaller in the unlensed source plane) but can achieve large boosts in sensitivity if positioned on the gravitational lensing critical line of a foreground galaxy cluster. The James Webb Space Telescope (JWST<sup>1</sup>), planned for launch in 2013, will have a better sensitivity, enabling observers to probe “pencil beams” out to even higher redshifts.

Recent data analysis from deep and narrow galaxy surveys have begun to incorporate theoretical models of structure formation and reionization. For example, Stark et al. (2007b) and Nagamine et al. (2008) have attempted to relate the observed UV and Lyman-alpha luminosities from these sources to the masses of the dark matter halos that host them by fitting the mass functions obtained from simulations and analytic prescriptions. In addition, Babich & Loeb (2006), McQuinn et al. (2007), and Wyithe & Loeb (2007) have proposed to study reionization by observing its effects on the galaxy power spectrum.

<sup>\*</sup> E-mail: jamunoz@cfa.harvard.edu

<sup>1</sup> <http://www.jwst.nasa.gov/>

In this paper, we study the underlying abundance and clustering statistics of halos in narrow fields-of-view. Our goal is to relate the theory of structure formation to the large amount of observational data from high-redshift galaxy surveys. We take into account the effect of large-scale density fluctuations as well as the nonlinearities on small scales. We use state-of-the-art numerical simulations to examine the field-to-field sample distribution and one-dimensional power spectrum of “pencil-beam” galaxy surveys that are much longer along the line-of-sight than across the field-of-view. Our analysis is designed to help observers in the interpretation of related observational data in the future.

Our paper is organized as follows. In §2 we describe our simulations. The probability distributions of object counts in high-redshift pencil surveys are analyzed in §3. In §4, we explore the one-dimensional power spectrum obtained from such surveys, the nonlinear bias, and the usefulness of such measures in relating galaxy luminosity and halo mass. Finally, we discuss our results and their implications for observations in §5.

## 2 THE SIMULATION DATA

To simulate observations of high-redshift galaxies, we adopt halo catalogs from an N-body simulation and semi-analytically dress each halo with a luminosity based on its mass. These catalogs were produced by the simulation used in Trac et al. (2008) which resolved halos with masses as low as  $\sim 10^8 M_\odot$  in a box of comoving size  $100 h^{-1}$  Mpc. This approach allows us to probe the faintest high-redshift galaxies within a sufficiently large simulation box that includes the important large-scale fluctuations. A flat,  $\Lambda$ CDM cosmology was assumed with cosmological parameters from the *Wilkinson Microwave Anisotropy Probe* 5-year data release,  $(\Omega_m, \Omega_\Lambda, \Omega_b, h, \sigma_8, n_s) = (0.28, 0.72, 0.046, 0.70, 0.82, 0.96)$ .

We determined a UV or Lyman- $\alpha$  luminosity for each halo in the simulation according to the prescription of Stark et al. (2007b). For LAEs, we chose the duty-cycle and the star formation efficiency to be  $\epsilon_{DC} = 1.0$  and  $f_* = 0.063$ , respectively. We adopted  $\epsilon_{DC} = 0.25$  and  $f_* = 0.16$  for LBGs. Since  $\epsilon_{DC} < 1$  for LBGs, we appropriately consider only a fraction,  $\epsilon_{DC}$ , of them to be observed in each snapshot of a galaxy survey.

## 3 PROBABILITY DISTRIBUTION OF GALAXY COUNTS

In this section we create mock samples of LBGs in pencil beams surveys at different redshifts. Since photometric redshifts of LBGs are typically imprecise, we consider groups of these galaxies in the redshift intervals of  $z = 6-8$  and  $z = 8-10$ . Many LBGs already have been observed in the HUDF around  $z = 6$  (Bouwens & Illingworth 2006; Bouwens et al. 2006), but observers have not yet had the same success at higher redshifts (Bouwens et al. 2008, 2009). Given its higher sensitivity, it is hoped that JWST will be able to observe LBGs at these redshifts.

To construct our samples of LBGs, we stitch together many simulation slices in the given redshift range so that

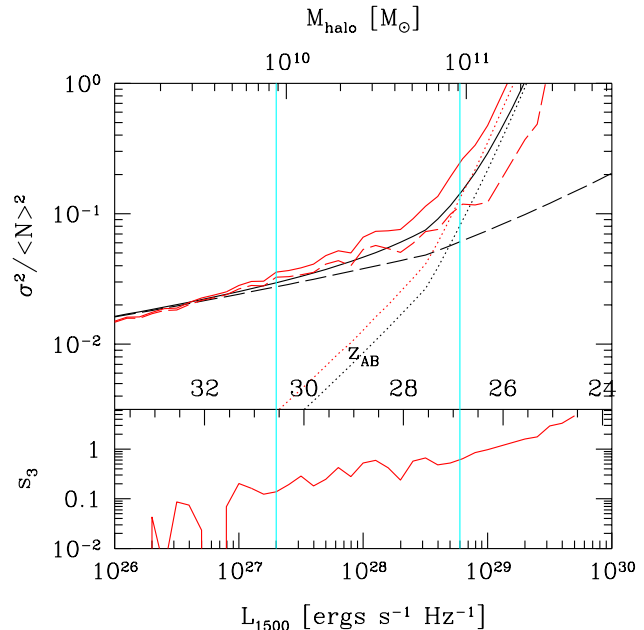


**Figure 1.** The upper panel shows relative contributions to the fractional variance in the number counts of galaxies as a function of UV luminosity, z-band magnitude, or host halo mass in counts of LBGs in a dropout survey spanning the redshift interval  $z = 6-8$  with a  $3.4' \times 3.4'$  field-of-view. Solid lines show the total variance, while long-dashed and dotted lines show the contributions from sample variance and Poisson noise, respectively. Red curves show simulation results, while black curves were calculated analytically. Vertical lines bracket the region where the variance is higher than expected due to the skewness of the full count probability distribution but is not Poisson-dominated. The lower panel shows the skewness of the full galaxy count probability distribution calculated from the simulation (Eq. 3).

each survey volume is viewed along the light-cone. This allows the mass function of halos to evolve along the line-of-sight, as needed to represent high-redshift surveys and to correctly analyze their statistics (Muñoz & Loeb 2008). For simplicity, we have assumed a top-hat selection function over each redshift interval.

For each redshift range, we compare the field-to-field variance in the count of LBGs in a “pencil beam” with a  $3.4' \times 3.4'$  field-of-view (equivalent to the HUDF and similar to that of JWST) determined from our simulation data. The sample variance according to linear perturbation theory (i.e. the variance from field to field based on the linear power-spectrum,  $P(k)$ ) in the abundance of halos with mass greater than  $M$  is:

$$\sigma_{hh}^2(M) = \frac{(b_{eff}(M) D(z))^2}{(2\pi)^3} \int P(k) W_{xyz}^2 d^3\vec{k}, \quad (1)$$

where  $W_{xyz} = W(k_x) W(k_y) W(k_z)$ ,  $k = \sqrt{k_x^2 + k_y^2 + k_z^2}$ ,  $D(z)$  is the linear growth factor evaluated, for simplicity, at the midpoint of the given redshift range, and  $b_{eff}$  is the Sheth et al. (2001) linear bias integrated over all masses above  $M$  and weighted by the Sheth & Tormen (1999) (hereafter ST) halo mass function (Matarrese et al. 1997; Muñoz & Loeb 2008). The window function,  $W(k_i)$ , is the Fourier transform of a top-hat in the  $i$ -th dimension and is

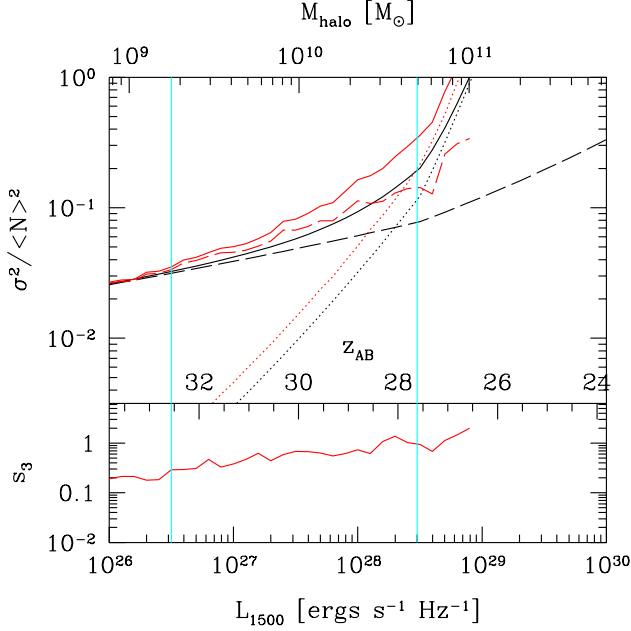


**Figure 2.** Same as Figure 1 but for the redshift interval  $z = 8-10$ .

given by:

$$W(k_i) = \frac{\sin(k_i a_i/2)}{k_i a_i/2}. \quad (2)$$

In equation (2),  $a_x = a_y = 3.4' (\pi/180 \times 60') \chi(z)$  are the narrow dimensions of the skewer-shaped survey evaluated at  $z$ . The subscript  $w$  refers to coordinates along the line-of-sight. The length of the survey,  $a_w$ , is given by the comoving distance between the limits bracketting the redshift range of interest.

The contribution to the variance from Poisson fluctuations is  $\sigma_P^2 = \langle N \rangle$ , where  $\langle N \rangle$  is the mean number of LBGs in each skewer. According to linear theory, the probability distribution of the count of LBGs is a Gaussian with variance given by the sum of the cosmic and Poisson contributions.

Figures 1 and 2 show the variance comparisons for the  $z = 6-8$  and  $z = 8-10$  ranges, respectively. They suggest that the observed statistics are well approximated by the analytic calculations at the low luminosity limits. However, analysis of the probability distribution of bright LBGs implies a non-Gaussian shape to the simulation data. This can be clearly seen in Figure 3, where the solid histogram representing the measured probability distribution is most closely fit by a log-normal distribution. The skewness as a function of minimum luminosity is presented in the bottom panels of figures 1 and 2. We define the skewness as the third moment of the probability distribution normalized by the variance to the 3/2 power:

$$s_3 = \frac{\langle (N - \langle N \rangle)^3 \rangle}{(\sigma^2)^{3/2}}. \quad (3)$$

The seemingly large amplitude variations in the skewness at low luminosity for  $z = 6-8$  are due to small numerical fluctuations around the nearly zero skewness from the simulation, plotted on a log scale. Deviations between the analytic and simulation values of the sample variance grow

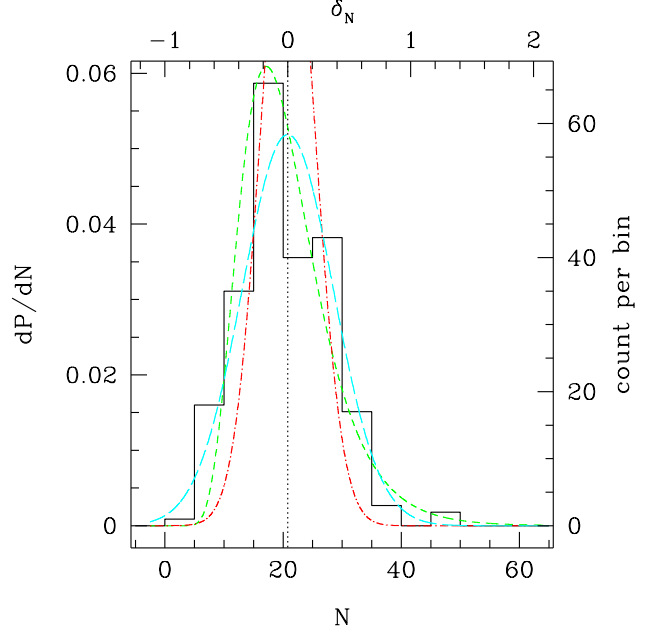


**Figure 3.** The full probability distribution for the number  $N$  of LBGs in a dropout survey spanning the redshift interval  $z = 8-10$  with a minimum galaxy luminosity of  $10^{28}$  ergs/s/Hz. The solid black curve shows the distribution as a histogram measured from the simulation, while the red dot-dashed, cyan long-dashed, and green short-dashed lines overlay Poisson, Gaussian, and log-normal distributions with the same mean, mean and standard deviation, and log-mean and log-standard deviation, respectively. The vertical, dotted line denotes the mean number of objects in the survey over many pointings. The distributions are plotted as differential probability in a differential abundance bin on the right, vertical axis as a function of the measured abundance of LBGs,  $N$ , on the lower, horizontal axis and as a function of the overdensity in the abundance  $\delta_N = N/\langle N \rangle - 1$  on the upper, horizontal axis. Additionally, the counts of pointings per abundance bin for the simulation histogram is shown on the right, vertical axis. These counts per bin show that Poisson errors in the simulation histogram are smaller than the differences between the overlaid distributions. The simulation results match most closely with the skewed log-normal distribution.

as the skewness becomes more significant. This behavior is a manifestation of nonlinear clustering on the small scales probed by the narrowness of the skewer.

Finally, the figures show sharp regimes where the field-to-field variance is dominated either by cosmic or Poisson variance. For the two redshift ranges  $z = 6-8$  and  $z = 8-10$  this division comes at around  $L(M = 9 \times 10^{28} M_{\odot}) = 6 \times 10^{28}$  ergs/s/Hz and  $L(M = 5 \times 10^{10} M_{\odot}) = 3 \times 10^{28}$  ergs/s/Hz, respectively. The nonlinearity at higher luminosities causes the sample variance to dominate at masses which are  $\sim 50-100\%$  larger than otherwise expected. However, since the Poisson variance is unaffected by nonlinearities, there remains only a specific mass range (shown in the figures) over which the total variance is different than expected.

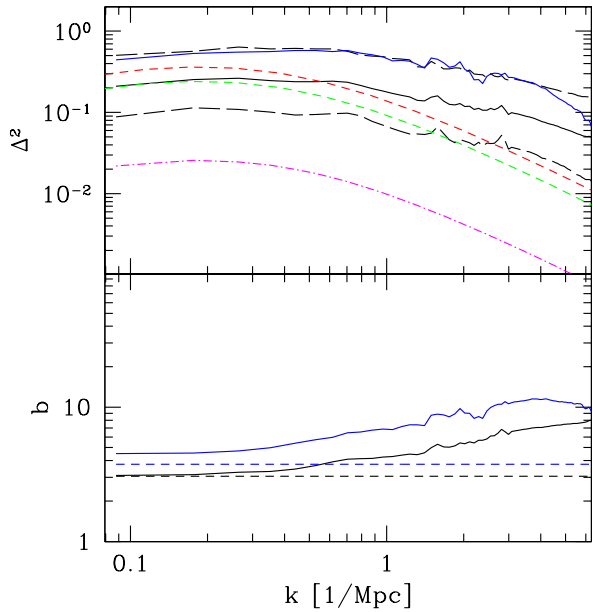


**Figure 4.** The 1D power spectrum of halos hosting LAEs in a survey with a  $3.4' \times 3.4'$  field-of-view at  $z = 6$ . The black (blue) lines represent values for a minimum Lyman- $\alpha$  luminosity of  $L_{L\alpha, \min} = 10^{40}$  ( $10^{41}$ ) ergs/s corresponding to  $M_{\text{halo}} = 1.6 \times 10^9$  ( $6.4 \times 10^9$ )  $M_{\odot}$ . In the upper panel, solid lines show the average log of the Poisson-subtracted, dimensionless power spectrum. Long-dashed lines indicate the estimated  $1 - \sigma$  variation in the log of the amplitude of the power spectrum from skewer-to-skewer. For clarity, these lines only appear for the lower luminosity threshold, but they are about the same size for the higher luminosity one. Short-dashed, green and red lines show the linear theory predictions for the dimensionless halo power spectrum given the lower and higher luminosity thresholds, respectively, while the dotted-dashed, magenta curve shows the linear theory calculations for the dark matter. The lower panel shows the non-linear bias (Eq. 7) measured from the simulation (solid lines) and the linear, ST bias (short-dashed lines).

#### 4 LINE-OF-SIGHT (ONE-DIMENSIONAL) POWER SPECTRUM

Next, we consider the one-dimensional (1D) galaxy power spectrum measured along the line-of-sight of a “pencil-beam” survey at high redshift with the same  $3.4' \times 3.4'$  field-of-view considered in the previous section. We explore what the information along the radial direction can or cannot tell us about the nature of high-redshift galaxies given the narrow field-of-view. We also examine whether or not it can be used to distinguish between luminous galaxies hosted by different mass halos, and ultimately to probe reionization. We are considering the “galaxy” power spectrum in the sense that we apply a duty cycle for LAEs and translate halo masses into hosted Lyman- $\alpha$  luminosities, but our results do not include the effects of reionization on the power spectrum that we expect to observe in real surveys (Babich & Loeb 2006; McQuinn et al. 2007; Wyithe & Loeb 2007).

When analyzing the 1D power spectrum, we do not attempt to produce mock surveys viewed along the light-cone since we wish to study the bias of the halos hosting high-redshift galaxies and compare our results to analytic, linear

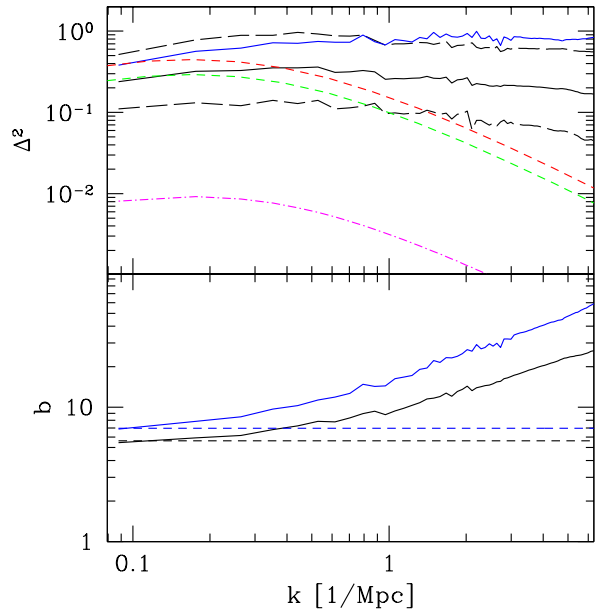


**Figure 5.** Same as Figure 4 except at  $z = 10$ . The minimum Lyman- $\alpha$  luminosity of  $L_{L\alpha, \min} = 10^{40}$  ( $10^{41}$ ) ergs/s corresponds to  $M_{\text{halo}} = 8.2 \times 10^8$  ( $3.2 \times 10^9$ )  $M_{\odot}$  at this redshift.

theory. For this purpose, it is preferable that the evolution of the halo mass and correlation functions will not introduce features in the power spectrum (Muñoz & Loeb 2008). Additionally, stitching together simulation slices to produce a view along the light-cone would unnecessarily add or subtract (depending on the prescription used) power from the spectrum on scales larger than the size of the simulation box and on the scale of the separation between simulation slices. As shown in Figures 4 and 5, the  $100 h^{-1}$  Mpc comoving size of the simulation box is sufficiently large to reproduce the linear results on the largest scales.

We calculate the spectrum in terms of real-space wave-numbers, as opposed to ones in redshift-space, and ignore contamination of distance measurements by peculiar velocities since they are expected to be small in the early universe. The redshift of LAEs can be constrained to within a few hundred km/s, corresponding to a wave-number of  $k \sim 3 \text{ Mpc}^{-1}$ , while the distances to high-redshift LBGs can be uncertain to hundreds of comoving Mpc (Bouwens & Illingworth 2006).

We compare the power spectrum calculated from the simulation using a 1D Fast Fourier Transform (FFT) to that determined analytically from linear perturbation theory. The theoretical 1D power spectrum is obtained by integrating the 3-dimensional power spectrum over a window function corresponding to the field-of-view (Kaiser & Peacock 1991):

$$P_{1D}(k_w, M) = \frac{(b_{\text{eff}}(M) D(z))^2}{(2\pi)^2} \int P(k) W_{xy}^2 dk_x dk_y, \quad (4)$$

where  $M$  is the minimum halo mass of the LBGs under consideration,  $k = \sqrt{k_x^2 + k_y^2 + k_w^2}$ ,  $W_{xy} = W(k_x) W(k_y)$ , and  $W(k_i)$  is the same as in equation 2. The power measured in the simulation, however, includes an additional, scale-independent component from Poisson noise. This, too, can

be calculated analytically as

$$P_{1D,Poisson}(M) = (\bar{n}( > M) a_x a_y a_w Q(a_w))^{-1} \quad (5)$$

and subtracted off, where  $\bar{n}( > M)$  is the ST halo mass function of LAE hosts with mass greater than  $M$  and

$$Q(a_w) = \frac{1}{2\pi} \int_{-\infty}^{\infty} W^2(k_w) dk_w. \quad (6)$$

Here,  $a_z$  can be any length scale and represents the depth of the skewer for which  $\sigma_P^2 = \langle N( > M) \rangle = \bar{n}( > M) a_x a_y a_w$  is the Poisson variance in the number of LAEs. Since,

$$\int_{-\infty}^{\infty} W^2(k_w) dk_w \sim 2/a_w,$$

$Q(a_w) \propto 1/a_w$ , and so  $P_{1D,Poisson}(M)$  is approximately independent of  $a_w$ , as expected. From equation 4, we can see that the 1D power spectrum at a given scale is a complicated convolution of shorter wavelength modes with the window function. This integration washes out any features that may have existed at small scales. Thus, we expect the 1D spectrum to be relatively featureless and smooth.

Figures 4 and 5 compare analytic and simulation calculations of the 1D power spectrum and bias after cosmic reionization is assumed to be completed ( $z = 6$ ) and in its early stages at  $z = 10$ , respectively. In both figures, the black (blue) lines represent values for a minimum Lyman- $\alpha$  luminosity of  $L_{L\alpha,min} = 1.6 \times 10^9$  ( $6.4 \times 10^9$ ) ergs/s corresponding to  $M_{halo} = 1.6 \times 10^9$  ( $6.4 \times 10^9$ )  $M_\odot$  at  $z = 6$  and  $M_{halo} = 8.2 \times 10^8$  ( $3.2 \times 10^9$ )  $M_\odot$  at  $z = 10$ . While LAEs are currently detected to approximately this luminosity at  $z = 6$ , future surveys should be able to probe down to the same luminosity at  $z = 10$ . Solid lines show the average log of the Poisson subtracted power spectrum (represented as  $\Delta^2(k) = k P_{1D}(k)/\pi$ ) measured from  $3 \times 17^2$  and  $3 \times 15^2$  skewers for  $z = 6$  and  $z = 10$ , respectively. The factor of 3 comes from additional independent skewers we obtained from rotating the simulation box.

Long-dashed lines indicate the estimated  $1 - \sigma$  variation in the log of the amplitude of the power spectrum from skewer-to-skewer. For clarity, these lines are only shown for  $L_{L\alpha,min} = 10^{40}$  ergs/s, but they are about the same size for  $L_{L\alpha,min} = 10^{41}$  ergs/s. An estimate of the power from a single skewer will fall within the  $1 - \sigma$  bounds 68 percent of the time. The standard deviation of the log of the power is approximately the same for all redshift and luminosity threshold combinations we considered with  $\sigma \approx 0.4$ ; it is also approximately independent of scale. Given this standard deviation and the number of independent skewers, the standard error in our estimate of the mean of the log of the power is  $\sigma_e = \sigma/\sqrt{N_{skewers}} \approx 0.02$ , where we have assumed that our estimate of the standard deviation is close to the true value.

The level of error in measuring the power informs whether the 1D power contains sufficient information to distinguish between galaxies of different masses and luminosities. This differentiability is important in constraining the mass-luminosity relationship and happens when  $\mu_{41} - \mu_{40} = 2(\sigma_{41} + \sigma_{40})/\sqrt{N_{skewers}}$ , where  $\mu_x$  and  $\sigma_x$  are the mean and standard deviations of the log of the power for the luminosity thresholds corresponding to  $L_{L\alpha,min} = 10^x$  ergs/s, and  $N_{skewers}$  is the number of independent fields-of-view (in this case all having dimensions of  $3.4' \times 3.4'$ ). On the largest

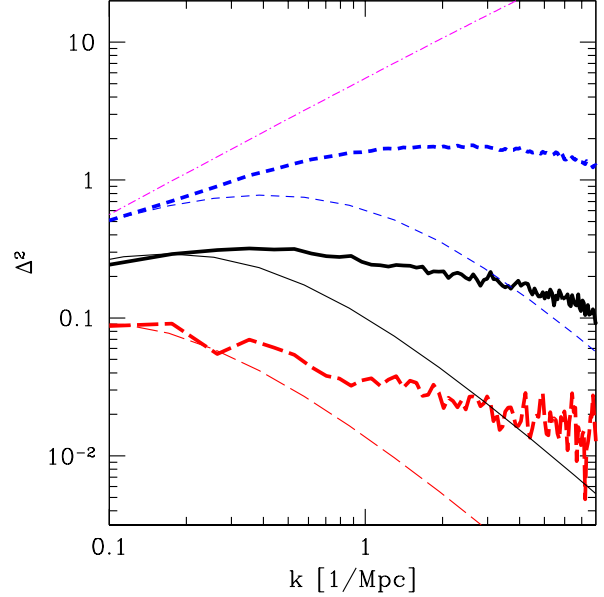


**Figure 6.** A comparison of the 1D power spectrum of halos hosting LAEs, as in Fig. 5, in surveys with different fields-of-view at  $z = 10$ . We set  $L_{L\alpha,min} = 10^{40}$  ergs/s for each survey. Thick lines show the simulated average log of the Poisson-subtracted, dimensionless power spectrum, while thin ones represent calculations from linear theory. Solid, black lines correspond to a  $3.4' \times 3.4'$  field-of-view, while the short-dashed, blue and long-dashed, red lines denote  $1' \times 1'$  and  $10' \times 10'$  fields-of-view, respectively. The field-to-field variance from Figures 4 and 5 have been omitted for clarity. For reference, we have plotted the linear theory spectrum for the dark matter assuming a pure 1D survey with an infinitesimal field-of-view as the dotted-dashed, magenta curve.

scales probed, the mean of the log of the power differs by  $\approx 0.23$  for both redshifts (with a weak redshift dependence). Thus, approximately 50 independent skewers are needed to distinguish between the two luminosity thresholds based on their 1D power spectrum.

The short-dashed green (red) line shows the analytic power-spectrum according to linear perturbation theory, with the same luminosity threshold as the black (blue) line. With no fit other than the calculations described above, the analytic predictions match the data from the simulations quite well on the largest scales. As soon as nonlinearities dominate on small scales, the simulation results and the analytic calculations diverge in their predictions. However, it is important to note that the nonlinearities at work are on even smaller scales than the deviation scale due to aliasing.

In the bottom panels of Figures 4 and 5, we show the halo bias,

$$b = \sqrt{P_{1D,halo}^{halo}/P_{1D,dm}^{analytic}}, \quad (7)$$

measured from the simulation (solid lines) and compare the results to the analytic ST calculation (short-dashed lines). Here,  $P_{1D,dm}^{analytic}$  is the linear, analytic calculation of the 1D dark matter power from equation (4) with  $b_{eff}(M) = 1$ . These plots show the same trend as in the upper panels with increasing divergence between simulation and analytic calculations on small scales. This is precisely the result ob-

tained from the full three-dimensional power by Trac & Cen (2007). However, note that the linear and nonlinear values do not match up exactly for  $L_{L\alpha, \min} = 10^{41}$  ergs/s at  $z = 6$ . The ST mass function is not a perfect fit over all masses and so it results in a slight deviation in the derived bias. This effect also manifests itself in the upper panel as a small deviation on large scales between the simulation and analytic power for the same luminosity and redshift.

A striking aspect of the 1D power spectrum illustrated in the top panels is that, for the  $3.4' \times 3.4'$  field-of-view, it remains relatively flat and featureless over a range of  $k$ -values spanning an order-of-magnitude or more. This smoothness is expected since both the aliasing of small-scale power and the averaging of many skewers wash out small features in the spectrum. However, the flatness is unique to our choice of field-of-view.

In Figure 6, we investigate how observational results from different fields-of-view can be compared by plotting the 1D power simulated in  $3.4' \times 3.4'$  pencil-beam skewers alongside those using  $1' \times 1'$  and  $10' \times 10'$  fields-of-view. The behavior in the interesting range of modes differs among the three cases because of the different modes allowed in the integration by the window function, which mixes up modes in a way that cannot be easily de-convolved (see Eq. 4).

Comparing the the linear theory predictions, we see that the position of the turn-over is directly related to the size of the window function with the narrower field-of-view turning over at larger  $k$ . Although the simulated position of the turn-over still increases monotonically with field-of-view size, the aliasing of nonlinear small-scale power changes the window function convolution in such a way that the position of the peak is not easily determined from the linear case.

It is also clear that the flatness we noted in the simulated spectrum for the  $3.4' \times 3.4'$  field-of-view is not generic; the spectrum for the narrowest field-of-view first rises with  $k$  and then decreases. The  $10' \times 10'$  field-of-view produces a spectrum that is flatter than the one produced by the  $1' \times 1'$  field-of-view, but since the peak is also at much larger scales, we end up probing the spectrum in the regime where it begins to fall off at small scales. The extra bumps and wiggles in the curve result from fewer skewers of that size being available for averaging.

For reference, we have also shown in Figure 6 the 1D dark matter power spectrum in an idealized 1D survey with an infinitesimal field-of-view. The aliased power in this case increases the amplitude of the spectrum even more than the bias factor in the LAE spectra using realistic fields-of-view. The figure shows the 1D power approaching this limit as the field-of-view for realistic surveys decreases.

## 5 CONCLUSIONS

In this work we have analyzed the statistics of galaxies in mock “pencil beam” surveys of high-redshift LBGs and LAEs with narrow fields-of-view produced using N-body simulations. We computed the effect of sample variance and nonlinear bias and showed how these will influence measurements of galaxy counts in existing and upcoming surveys.

While the variance due to fluctuations in the local overdensity in LBG surveys increases almost monotonically with increasing luminosity (or halo mass), it dominates only at

low luminosities and is overtaken at high luminosities by a Poisson variance that rises more steeply as the average number of galaxies in the survey drops. However, the overdensities become nonlinear on small scales. A given point is more likely to be in underdense regions than in overdense regions because of their larger volume filling fraction. The resulting skewness of the probability distribution of galaxy counts creates slightly more uncertainty in obtaining the true number density of galaxies at the observed redshift than would otherwise be expected. This can be seen graphically in Fig. 3 where the simulation histogram is most closely matched by a skewed, log-normal distribution whose peak is centered on negative values of the overdensity. The skewness of the distribution and the resulting increased probability of surveying an underdense region should be taken into account when interpreting galaxy counts in the context of the ionizing UV background they produce at high redshift, or else it would result in an underestimate of the background. Precise measurements of the cosmic variance in a survey is also important for understanding the differences between two independent samples. Our results and methods can be used to calibrate these errors for different fields-of-view and survey depths appropriate to a given study instead of relying only on linear theory estimates at a single redshift as in Bouwens et al. (2008).

Whether or not future surveys of LAEs will have the angular resolution to compute angular correlation functions in the plane of the sky, they will probe many more modes along the line-of-sight. We expect the 1D power spectrum from surveys with a JWST-sized field-of-view to exhibit a roughly flat, smooth profile. Aliasing and the averaging of many skewers are expected to result in a relatively featureless spectrum unable to probe void structure like that seen in Broadhurst et al. (1990). The flatness, on the other hand, is unique to the particular choice of field-of-view, and comparing JWST results, such as measurements of the galaxy bias, with those from other surveys will not be trivial due to the complicated convolution with the window function. Nonetheless, if the survey parameters are known, the amplitude on the largest scales matches well with the expectation from linear theory. However, on small scales, the nonlinear bias becomes large. Given their limited fields-of-view, a survey with JWST will need tens of pointings to be able to distinguish between host halo masses different by an order-of-magnitude limiting its usefulness in determining their mass-to-light ratios. Finally, our calculations ignored the complex effects of reionization on the amplitude of the power spectrum. The mass-to-light ratio for LAEs at redshifts during reionization could first be calibrated by extrapolating determinations made after reionization, through either clustering or abundance matching. With this information in hand, differences between our results and observations will show the effect of Lyman- $\alpha$  transmission through the HII regions around ionizing sources. However, probing reionization through the changing amplitude of the 1D spectrum (McQuinn et al. 2007) will require particular consideration of the field-of-view.



## 6 ACKNOWLEDGEMENTS

We would like to thank Mark Dijkstra for useful discussions. This research was supported in part by NASA grants NNX08AL43G and LA and by Harvard University funds.

## REFERENCES

- Babich, D., & Loeb, A. 2006, *ApJ*, 640, 1
- Barkana, R., & Loeb, A. 2001, *Physics Reports*, 349, 125
- Bouwens, R., & Illingworth, G. 2006, *New Astronomy Review*, 50, 152
- Bouwens, R., Illingworth, G., Blakeslee, J., & Franx, M. 2006, *ApJ*, 653, 53
- Bouwens, R. J., Illingworth, G. D., Bradley, L. D., Ford, H., Franx, M., Zheng, W., Broadhurst, T., Coe, D., & Jee, M. J. 2009, *ApJ*, 690, 1764
- Bouwens, R. J., et al. 2008, *ApJ*, 686, 230
- Broadhurst, T. J., Ellis, R. S., Koo, D. C., & Szalay, A. S. 1990, *Nat*, 343, 726
- Gnedin, N. Y., & Kravtsov, A. V. 2006, *ApJ*, 645, 1054
- Kaiser, N., & Peacock, J. A. 1991, *ApJ*, 379, 482
- Kravtsov, A. V., & Gnedin, O. Y. 2005, *ApJ*, 623, 650
- Madau, P., Kuhlen, M., Diemand, J., Moore, B., Zemp, M., Potter, D., & Stadel, J. 2008, *ApJ*, 689, L41
- Matarrese, S., Coles, P., Lucchin, F., & Moscardini, L. 1997, *MNRAS*, 286, 115
- McQuinn, M., Hernquist, L., Zaldarriaga, M., & Dutta, S. 2007, *MNRAS*, 381, 75
- Mobasher, B., Dickinson, M., & Ferguson, H. C. 2005, *ApJ*, 635, 832
- Moore, B., Diemand, J., Madau, P., Zemp, M., & Stadel, J. 2006, *MNRAS*, 368, 563
- Muñoz, J. A., & Loeb, A. 2008, *MNRAS*, 386, 2323
- Muñoz, J. A., Madau, P., Loeb, A., & Diemand, J. 2009, *arXiv:astro-ph/0905.4744*
- Nagamine, K., Ouchi, M., Springel, V., & Hernquist, L. 2008, *arXiv:astro-ph/0802.0228*
- Richard, J., Stark, D. P., Ellis, R. S., George, M. R., Egami, E., Kneib, J.-P., & Smith, G. P. 2008, *ApJ*, 685, 705
- Sheth, R. K., Mo, H. J., & Tormen, G. 2001, *MNRAS*, 323, 1
- Sheth, R. K., & Tormen, G. 1999, *MNRAS*, 308, 119
- Stark, D. P., Ellis, R. S., Richard, J., Kneib, J.-P., Smith, G. P., & Santos, M. R. 2007a, *ApJ*, 663, 10
- Stark, D. P., Loeb, A., & Ellis, R. S. 2007b, *ApJ*, 668, 627
- Trac, H., & Cen, R. 2007, *ApJ*, 671, 1
- Trac, H., Cen, R., & Loeb, A. 2008, *ApJ*, 689, L81
- Wiklind, T., et al. 2008, *ApJ*, 676, 781
- Wyithe, J. S. B., & Loeb, A. 2006, *Nat*, 441, 322
- . 2007, *MNRAS*, 382, 921